Title

HIGH RESOLUTION OBSERVATIONS OF COPPER VACANCY ORDERING IN CHALCOCITE (Cu2S) AND THE TRANSFORMATION TO DJURLEITE (Cu1.97-1.94S)

Authors

Sands, T.D.
Washburn, J.
Gronsky, R.

Publication Date

1982

LBL-13746
Preprint

Lawrence Berkeley Laboratory
UNIVERSITY OF CALIFORNIA

Materials & Molecular Research Division

Submitted to Physica Status Solidi

HIGH RESOLUTION OBSERVATIONS OF COPPER VACANCY ORDERING IN CHALCOCITE (Cu_2S) AND THE TRANSFORMATION TO DJURLEITE ($Cu_{1.97-1.94}S$)

T.D. Sands, J. Washburn, and R. Gronsky

January 1982

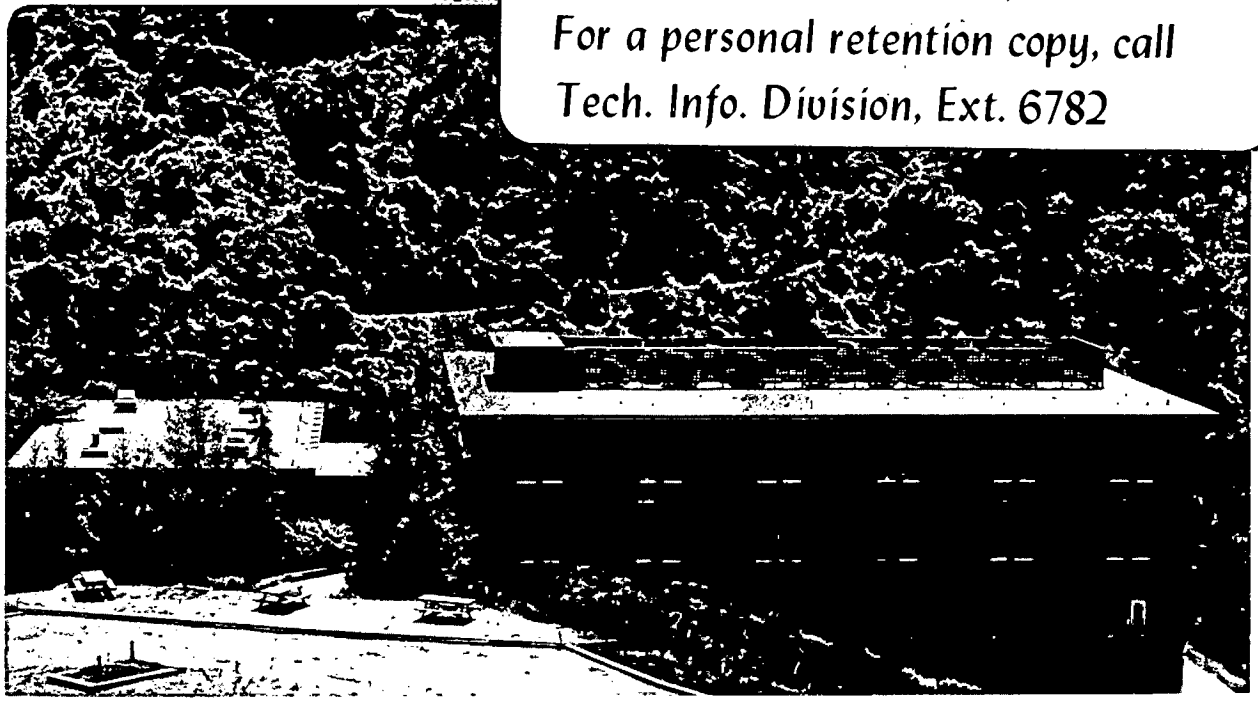

Prepared for the U.S. Department of Energy under Contract W-7405-ENG-48

DISCLAIMER

High Resolution Observations of Copper Vacancy Ordering in Chalcocite (Cu_2S) and the Transformation to Djurleite ($Cu_{1.97-1.94}S$)

by

T. D. Sands, J. Washburn and R. Gronsky
Materials and Molecular Research Division
Lawrence Berkeley Laboratory
University of California
Berkeley, CA 94720

The technique of high resolution transmission electron microscopy (TEM) has permitted the first real space observations of the ordering of copper in the sulfur sublattices of chalcocite (Cu_2S) and djurleite ($Cu_{1.97-1.94}S$). Copper sulfide thin films formed by the ion exchange process in CdS single crystals are shown to be composed of small domains of the two phases (~ 10 to 100nm in diameter), separated by abrupt coherent interfaces. Strain calculations for these interfaces agree qualitatively with experimental observations. In addition, the chalcocite in the vicinity of chalcocite/djurleite interfaces was found to contain a high density of 1/4[010] faults. Structural considerations show that these faults are likely sites for copper vacancies.

1. Introduction

$Cu_{2-x}S$/(Cd,Zn)S thin film photovoltaic devices have recently surpassed 10% efficiency in the lab [1]. Unfortunately, the feasibility of these devices for terrestrial use is limited by inherent instabilities in the copper sulfide layer [1 → 4]. Extended heat treatments [2], exposure to the atmosphere [5 → 8], and field-assisted copper migration [4,7,8] can all result in the transformation of chalcocite ($\sim Cu_{1.995}S$) to djurleite ($Cu_{1.97-1.94}S$) with a corresponding reduction in cell efficiency [9,10]. The development of a copper sulfide layer with improved stability and optimum stoichiometry has been inhibited by a lack of understanding regarding the structures and phase relationships of chalcocite and djurleite [11]. It is the objective of this study to determine the structural relationships between these two phases so that the low-temperature ($T < 100°C$) transformation mechanism may be determined.

1.1. Copper Sulfide Phase Relationships

Both chalcocite and djurleite are composed of an ordered superlattice of copper within a distorted hexagonal-close-packed sulfur sublattice. Above 104°C the copper atoms in Cu_2S become disordered. However, below 435°C the hexagonal-close-packed sulfur sublattice is retained [12-14]. This disordered phase is hexagonal (space group $P6_3/mmc$) with $a_{hex} = .395nm$ and $c_{hex} = .675nm$ [11].

Equilibrium phase diagram determination has been hampered by the appearance of several metastable phases and the kinetic effects associated with them [12,14]. The most accurate results to date have come from electrochemical measurements by Potter [12]. His version of the Cu-S phase diagram (Fig. 1) illustrates the extreme structural

sensitivity of $Cu_{2-x}S$ to small deviations in stoichiometry from $Cu_{2.000}S$, especially near the order-disorder transition temperatures (90-104°C).

The structure of the stable low temperature phases, djurleite and low chalcocite, are still in question. However, x-ray work by Evans [15,16] has yielded results which are reasonable but complicated. Evans found that low chalcocite is monoclinic with a space group of either $P2_1/c$ or Pc and the following unit cell parameters:

a = 1.525nm

b = 1.188nm

c = 1.349nm

β = 116.35°

cell content: 48 Cu_2S.

The c-axis coincides with the c-axis of the sulfur sublattice while b is approximately three times the hexagonal sublattice parameter "a_{hex}". Djurleite ($Cu_{1.938}S$) was also found to be monoclinic with space group $P2_1/n$ and the following unit cell parameters:

a = 2.690nm

b = 1.575nm

c = 1.357nm

β = 90.13°

cell content: 248 Cu, 128 S.

The a-axis coincides with the c-axis of the sulfur sublattice while b is approximately four times the hexagonal sublattice parameter "a_{hex}".

Electrochemical measurements by Potter [12] indicate that djurleite is a solid solution with (2-x) varying from 1.965 to 1.934. Since one copper vacancy in the asymmetric unit of djurleite yields a composition of $Cu_{1.969}S$ while two vacancies yield a composition of $Cu_{1.938}S$, it is reasonable to consider djurleite to be a superstructure resulting from the ordering of copper vacancies in low chalcocite. The structure of $Cu_{1.969}S$ has not been reported, presumably because it is very difficult to isolate this phase from chalcocite and $Cu_{1.938}S$ [15] (as would be required for conclusive x-ray diffraction measurements). However, lattice parameter measurements by electron diffraction of Cu-rich djurleite coherently intergrown with chalcocite yield values similar to those reported by Evans for $Cu_{1.938}S$.*

The structural relationships between chalcocite and djurleite are difficult to visualize with the unit cells described above. Fortunately, both phases can be adequately described with simple pseudo-orthorhombic unit cells which clearly reveal geometrical relationships. Thus, the following approximate unit cell conventions will be used for the remainder of the paper:

chalcocite	a'	= 1.19nm
	b'	= 2.73nm
	c'	= 1.35nm
djurleite	a'	= 1.57nm
	b'	= 1.36nm
	c'	= 2.69nm

*For example see Fig. 7c

With these conventions the following relationships hold with respect to the lattice parameters of high-temperature hexagonal chalcocite:

chalcocite	a'	$\tilde{=} 3 . a_{hex}$
	b'	$\tilde{=} 4\sqrt{3} . a_{hex}$
	c'	$\tilde{=} 2 . c_{hex}$
djurleite	a'	$\tilde{=} 4 . a_{hex}$
	b'	$\tilde{=} 2\sqrt{3} . a_{hex}$
	c'	$\tilde{=} 4 . c_{hex}$.

From the above, it is evident that the pseudo-orthorhombic unit cells of both chalcocite and djurleite can have any of three orientations at ~ 120° intervals about the c-axis in a fixed h.c.p. sulfur sublattice (see Fig. 2). However, the distortion of the actual sulfur sublattice makes certain orientational combinations of the two phases more compatible than others (see Sec. 3.2).

1.2. Electron Microscopy of the Chalcocite-Djurleite Transformation

The structural compatibility of low chalcocite and djurleite, and the small difference in composition between these two phases makes macroscopic studies of their structure and transformations ambiguous. The chalcocite-djurleite transformation has not, to the author's knowledge, been studied previously in real space at a microscopic level. However, an electron diffraction experiment involving these phases has been reported by A. Putnis [11]. He observed the behavior of copper sulfide specimens of unknown composition when heated by the electron beam. As he monitored

electron diffraction patterns of the same areas through heating and cooling cycles, Putnis noted that the two phases, chalcocite and djurleite, seemed to form with nearly equal likelihood upon cooling, regardless of the initial phase. Putnis concludes: "The transformation sequence clearly implies that the chalcocite and djurleite superstructures can exist at the same chemical composition."

Although his results may be important, there is some question about the validity of his interpretation. First, as the results presented in this paper show, chalcocite and djurleite can be coherently intergrown with superlattice grain dimensions varying from ten nanometers to several hundred nanometers. Therefore, a two phase mixture, when heated above the order-disorder transformation temperature and then cooled, can have a resulting microstructure with an entirely different spatial arrangement of the two phases (requiring only a small amount of Cu ion movement), while preserving the same <u>average</u> composition.

Second, Putnis reports that he was able to monitor the diffraction pattern from the same 100nm diameter area through the thermal cycles using a selected area aperture. However, the uncertainty in locating a selected area aperture is typically 35nm (on the specimen plane) due to spherical aberration of the objective lens [17]. In addition, the necessary adjustment of the specimen position after beam heating introduces further uncertainties.

To avoid these difficulties and their associated ambiguities, the technique of phase contrast transmission electron microscopy was chosen to observe the microstructure of $Cu_{2-x}S$ in both real space and reciprocal space. An added benefit of this method is that TEM specimens are

generally several tens of nanometers to several hundred nanometers thick, approximately the same thickness range as that of typical $Cu_{2-x}S$ layers in $Cu_{2-x}S$/CdS solar cells.

2. Experimental

In order to avoid the complications of CdS grain boundaries in this initial study, bulk single crystals of undoped CdS (Eagle-Picher) were used as the starting material. Transmission electron microscope specimens of CdS were fabricated by orienting the crystal with the Laue x-ray technique ((0001) orientation), sectioning the CdS with a diamond saw, and then mechanically and chemically polishing the specimen to a thickness of approximately 50μm. The final thinning was accomplished by argon ion milling to electron transparency.

Freshly ion milled CdS specimens were etched for 5-10 seconds in 37% HCl and then dipped in a CuCl (5-9's) ion exchange bath [18] for 30 seconds at 95 to 98°C (the conventional method of preparing $Cu_{2-x}S$ layers for solar cells). The resulting topotaxial exchange reaction converted the entire thin area (transparent to 100keV electrons) to $Cu_{2-x}S$. A small concentration of cadmium trapped at the end of the exchange process probably remained in the copper sulfide, especially in the thicker regions of the specimens near the CdS/$Cu_{2-x}S$ interface [19].

Specimens were rinsed in de-ionized water to terminate the exchange reaction and remove surface reaction products (i.e. $CdCl_2$). After drying in air at room temperature for several hours, a $Cu_{2-x}S$/CdS specimen was inserted into a Siemens 102 transmission electron microscope operated at 100kV. Phase contrast electron microscopy was

used to obtain a "superstructure image"* of a desired area in a [001] zone axis orientation. Each specimen was re-examined after a heat treatment in laboratory air at 180 ± 5°C for several minutes (simulating heat treatments given to $Cu_{2-x}S$/CdS solar cells). Microstructural changes observed in the same areas after heat treatment are not the subject of this paper and will be reported elsewhere.

3. Results and Discussion

3.1. The Structures of Chalcocite and Djurleite.

Using the atom positions reported by Evans [15,16], the structures of chalcocite and djurleite can be compared as follows:

The low chalcocite structure has a fairly well-developed $Cu_{12}S_6$ repeat unit (see Fig. 3). The pseudo-orthorhombic unit cell contains 16 of these units. All have approximately the same structure although exact atom positions vary from one unit to the next. The prominent feature of these $Cu_{12}S_6$ groups is a ring of five copper atoms occupying five corners of a distorted hexagon.** The spatial arrangement of these building units is indicated in Fig. 4.

---

*Only superlattice reflections were admitted by the objective aperture. See Fig. 7a.

**The chalcocite structure reported by Evans [15,16] has eight building units per monoclinic unit cell. One unit has a four-Cu layer, one has a six-Cu layer, and the remaining units have five-Cu layers.

Examination of the djurleite ($Cu_{1.938}S$) structure did not reveal a repeating building unit which involves all of the atoms of the unit cell. However, "double building units" of composition $Cu_{20}S_{12}$ are located at body-centered sites of the pseudo-orthorhombic unit cell. These clusters resemble two chalcocite building units placed base-to-base. The major difference is that the two five-member rings are replaced by a single six-member ring (see Fig. 5). The remaining copper atoms in the unit cell are ordered in a manner similar to the ordering of copper in chalcocite.

The two $Cu_{20}S_{12}$ groups per unit cell account for all eight of the vacancies in a unit cell of djurleite ($Cu_{1.938}S$). The tendency for four vacancies to cluster into a $Cu_{20}S_{12}$ group and the fact that the lattice parameters of $Cu_{1.969}S$ and $Cu_{1.938}S$ are similar, lead to the conclusion that there is probably no radical difference between the structures of these two extremes of the djurleite solid-solution range. Therefore, it seems likely that the four vacancies per unit cell of $Cu_{1.969}S$ are all clustered into one $Cu_{20}S_{12}$ group with the remainder of the copper atoms ordered in groups similar to the building units of chalcocite.

3.2. Chalcocite/Djurleite Interfaces

The technique of high resolution TEM allows direct observation of chalcocite/djurleite interfaces. Fig. 6 schematically illustrates ten variations of vertical interfaces (containing the c'-axis). Each of the interfaces observed in this study fits into one of these ten categories.

Based on a reduction of strain energy alone, one would expect to observe mostly E(0.1%) or G(0.3%) interfaces. Accordingly, the most

common interface observed in this study was E (see Figs. 7c, 8 and 9) followed by G (Figs. 7c and 9). Close examination of Fig. 7c reveals an E, G interface which appears to be highly coherent and essentially strain-free (see Figs. 7a and 7b for indexed diffraction pattern). A lower magnification image of the same region shows that this interface is roughly flat for at least 100nm, considerably longer than any other chalcocite/djurleite boundary imaged in this study.

As expected, the higher mismatch interfaces (F = 1.0% and H = 1.2%) were observed infrequently and found to be short (~6nm) and highly strained (see Fig. 8). Correspondingly, the 0.6 to 0.7% mismatch interfaces imaged in Figs. 10 (B: 0.6%) and 11 (A: 0.7%) are intermediate in length (~ 10 to 20nm).

Observations of these interfaces after aging in air at room temperature indicate that the low temperature transformation proceeds by the motion of low strain interfaces (such as E and G) at the expense of higher strain regions (such as the island of djurleite imaged in Fig. 10). However, before observations of these interfaces can be properly interpreted, the nature of the faulting observed on (040) planes of chalcocite (Figs. 7c, 9 and 11) must be clearly understood.

3.3. Faulting in Chalcocite.

The frequently observed variation in spacing along the [010] direction in chalcocite is most easily explained by the 1/4 [010] fault diagrammed in Fig. 12. The 5-Cu layers of the $Cu_{12}S_6$ building unit are represented as in Fig. 12. Note that, in the unfaulted structure, a copper

atom is associated with each side of the hexagon. Therefore, each hexagon contains 4 + 1/2 + 1/2, or five, copper atoms. If this same rule is obeyed for the faulted structure in Fig. 17, then each hexagon along the fault contains an average of four copper atoms. Thus, the densely-packed copper layers along the fault are likely sites for copper vacancies (and possibly Cd^{++} impurities).

Further support for this model comes from the observation of these faults near chalcocite/djurleite interfaces. Vacancy condensation along these faults would slightly reduce the average S-S distance in the basal plane, thereby affording a better lattice match with djurleite. However, if the 5-Cu layers remained intact at the fault, the resulting expansive strain on the sulfur sublattice would increase the lattice mismatch between chalcocite and djurleite. Therefore, it seems spatially and energetically favorable for vacancies to condense on these chalcocite 1/4 [010] faults. In fact, comparison of faulted regions with adjacent unfaulted areas show that the fault width is approximately 8% smaller than the separation between (040) planes in unfaulted chalcocite (for example, lattice parameter measurements of the area imaged in Fig. 9 show that the fault width is 0.63 $\pm$ 0.03nm compared to the unfaulted (040) separation of approximately 0.68nm).

Perhaps the most interesting consequence of this model is the predicted variation in the copper-to-sulfur ratio allowed by these faults. Table 1 shows the calculated composition of chalcocite as a function of the average distance between faults along with the percent lattice contraction assuming an 0.05nm contraction per fault.

TABLE 1

CALCULATED COMPOSITIONS OF FAULTED CHALCOCITE

Spacing between faults in [010] direction	Lattice contraction in [010] direction	Composition (2-x)
3.4nm	1.5%	1.933
4.8	1.1	1.952
6.1	0.8	1.963
7.5	0.7	1.969
8.9	0.6	1.974
10.2	0.5	1.978
14.3	0.3	1.984
28.0	0.2	1.992
100.0	-	1.996

Note that a fault spacing of 7.5nm (equivalent to five 1.36nm wide unfaulted layers separating each 0.63nm wide faulted layer) yields a composition of $Cu_{1.969}S$, the copper-rich end of the djurleite solid solution range. This may explain the unexpected results obtained by Putnis (described in the Introduction) [11].

The verification of this model with further microscopy, including careful lattice parameter measurements, may allow the association of

compositional maps with high resolution images of chalcocite. Such maps would be very useful for quantifying the effects of environment on copper sulfide.

3.4. Model of the Chalcocite-Djurleite Transformation

Based upon the observations of the above sections, the following model of the low temperature oxidation of chalcocite to djurleite has emerged:

First, the relatively well-ordered chalcocite loses some copper to oxygen or CO_2 at a free surface or grain boundary. The high mobility of copper [20] allows groups of four Cu vacancies to readily cluster into $Cu_{20}S_{12}$ units. These clusters assume their lowest energy by ordering in an orthorhombic fashion with copper and sulfur atoms appearing in a two-to-one ratio surrounding the $Cu_{20}S_{12}$ groups. The resulting interface is between chalcocite and djurleite ($Cu_{1.969}S$).

Further copper removal at the chalcocite/djurleite boundary leads to the motion of this interface and the clustering of more copper vacancies into $Cu_{20}S_{12}$ groups. These additional clusters form at sites in body-centered positions of the unit cells of djurleite. A region saturated with these clusters has 8 copper vacancies per unit cell volume and a composition of $Cu_{1.938}S$, which is the composition of the djurleite studied by Evans [15]. Thus, djurleite may be regarded as a solid solution with a constant orthorhombic framework of $Cu_{20}S_{12}$ groups. Compositions between $Cu_{1.938}S$ and $Cu_{1.969}S$ can be achieved by a statistical distribution of $Cu_{20}S_{12}$ clusters among the body-centered sites. Copper

loss from $Cu_{1.938}S$ results in the formation of other phases which are beyond the scope of this investigation.

4. Conclusion

The microstructure of $Cu_{2-x}S$ is determined primarily by the ordering of copper vacancies. The high mobility of copper ions in the sulfur sublattice and the variability of their charge states facilitate the condensation of copper vacancies into planar 1/4 [010] faults in chalcocite and 4-vacancy clusters ($Cu_{20}S_{12}$ units) in djurleite. Consequently, the chalcocite-djurleite transformation involves short range diffusion of copper ions in the interface region.

Acknowledgements

This work was supported by the Director, Office of Energy Research, Office of Basic Energy Sciences, Division of Materials Sciences of the U. S. Department of Energy under Contract No. W-7405-ENG-48.

References

[1] J. Leong and S. Deb, SERI/TP-613-1220 (1981).

[2] L. C. Burton and H. M. Windawi, J. Appl. Phys. 47, 4621 (1976).

[3] B. G. Caswell and J. Woods, phys. stat. sol. (a) 44, K47 (1977).

[4] H. J. Mathieu, K. K. Reinhartz, and H. Rickert, 10th IEEE Photovoltaic Spec. Conf., 93 (1973).

[5] R. J. Mytton et al., 9th IEEE Photovoltaic Spec. Conf., 133 (1972).

[6] A. L. Fahrenbruch and R. H. Bube, 10th IEEE Photovoltaic Spec. Conf., 85 (1973).

[7] W. Palz et al., 10th IEEE Photovoltaic Spec. Conf., 69 (1973).

[8] H. M. Windawi, 11th IEEE Photovoltaic Spec. Conf., 464 (1975).

[9] J. Washburn and T. Peterson, phys. stat. sol. (a) 22, 721 (1974).

[10] N. Convers Wyeth and A. W. Catalano, 12th IEEE Photovoltaic Spec. Conf., 471 (1976).

[11] A. Putnis, Am. Mineralogist 62, 107 (1977).

[12] R. W. Potter, Economic Geology 72, 1524 (1977).

[13] W. R. Cook, L. Shiozawa, and F. Augustine, J. Appl. Phys. 41, 3058 (1970).

[14] E. H. Roseboom, Economic Geology 61, 641 (1966).

[15] H. T. Evans, Science 203, 356 (1979).

[16] H. T. Evans, Nature Phys. Science 232, 69 (1971).

[17] G. Thomas and M. J. Goringe, Transmission Electron Microscopy of Materials, (John Wiley and Sons, 1979), 27.

[18] B. Baron, A. W. Catalano and E. A. Fagen, 13th IEEE Photovoltaic Specialists.

[19] V. G. Bhide et al. J. Phys. D: Appl. Phys. 14, 1647 (1981).

[20] T. Kanashiro et al., Solid State Ionics 3/4, 327 (1981).

Figure Captions

Fig. 1. Cu-S phase diagram as determined by Potter [12]. "Ch_{dis}" represents disordered hexagonal chalcocite

Fig. 2. Chalcocite and djurleite psuedo-orthorhombic unit cells in the basal plane of the sulfur sublattice. The dotted line indicates the apparent size of the chalcocite unit cell in c'-axis projection.

Fig. 3. Exploded schematic diagram of the $Cu_{12}S_6$ chalcocite building unit. Sulfur atoms are in roughly h.c.p. positions.

Fig. 4. The arrangement of building units in chalcocite. Hexagons represent the five-Cu layers of the building units (see Fig. 3). The remainder of the unit is above (O) or below (O) the indicated plane.

Fig. 5. Exploded schematic diagram of the djurleite $Cu_{20}S_{12}$ four-vacancy cluster.

Fig. 6. Schematic representation of chalcocite/djurleite interfaces containing the c'-axis. Wider spaced lines represent the (100) planes of djurleite (~ 1.6nm spacing). Narrowly-spaced lines represent the (100) planes of chalcocite (~ 1.2nm spacing). The number below each diagram is the precent misfit in the sulfur basal plane calculated from the data of Evans [15,16]. The chalcocite sublattice is always larger.

Fig. 7a. Typical [001] zone axis chalcocite/djurleite diffraction pattern of as as-plated specimen. Note the streaks through the 020 position of the chalcocite reciprocal lattice. The

circular shadow represents the size of the objective aperture used throughout this study. Diffraction spots are indexed in Fig. 7b. Fig. 7c is the high resolution image corresponding to the diffraction pattern of Fig. 7a. Faults (three of which are indicated by arrows) are responsible for the streaking in the diffraction pattern.

Fig. 8 High strain chalcocite/djurleite interfaces. Note lobes of strain contrast due to an H (1.2%) interface (right arrow) and an F (1.0%) interface (left arrow).

Fig. 9. Two pairs of 1/4 [010] faults in chalcocite. One pair is separated by 3.4nm while the other pair is separated by 4.8nm.

Fig. 10. Island of djurleite surrounded by chalcocite.

Fig. 11. 1/4 [010] fault near chalcocite/djurleite interface.

Fig. 12. Diagram of chalcocite 1/4 [010] fault. For simplicity, the fault width is shown as half of the (020) spacing. Measurements indicate that the true fault width is 0.63 $\pm$ 0.03nm. As in Fig. 4, hexagons represent the densely packed copper layers of the chalcocite building units. Units which have their five-Cu layers 0.34nm above and below the indicated plane occupy the space between each row of hexagons. One copper atom is associated with each unshared side of a hexagon. Shared sides also contain one copper atom, resulting in the five-Cu layers of the unfaulted chalcocite and the predicted nonstoichiometry of the faulted chalcocite.

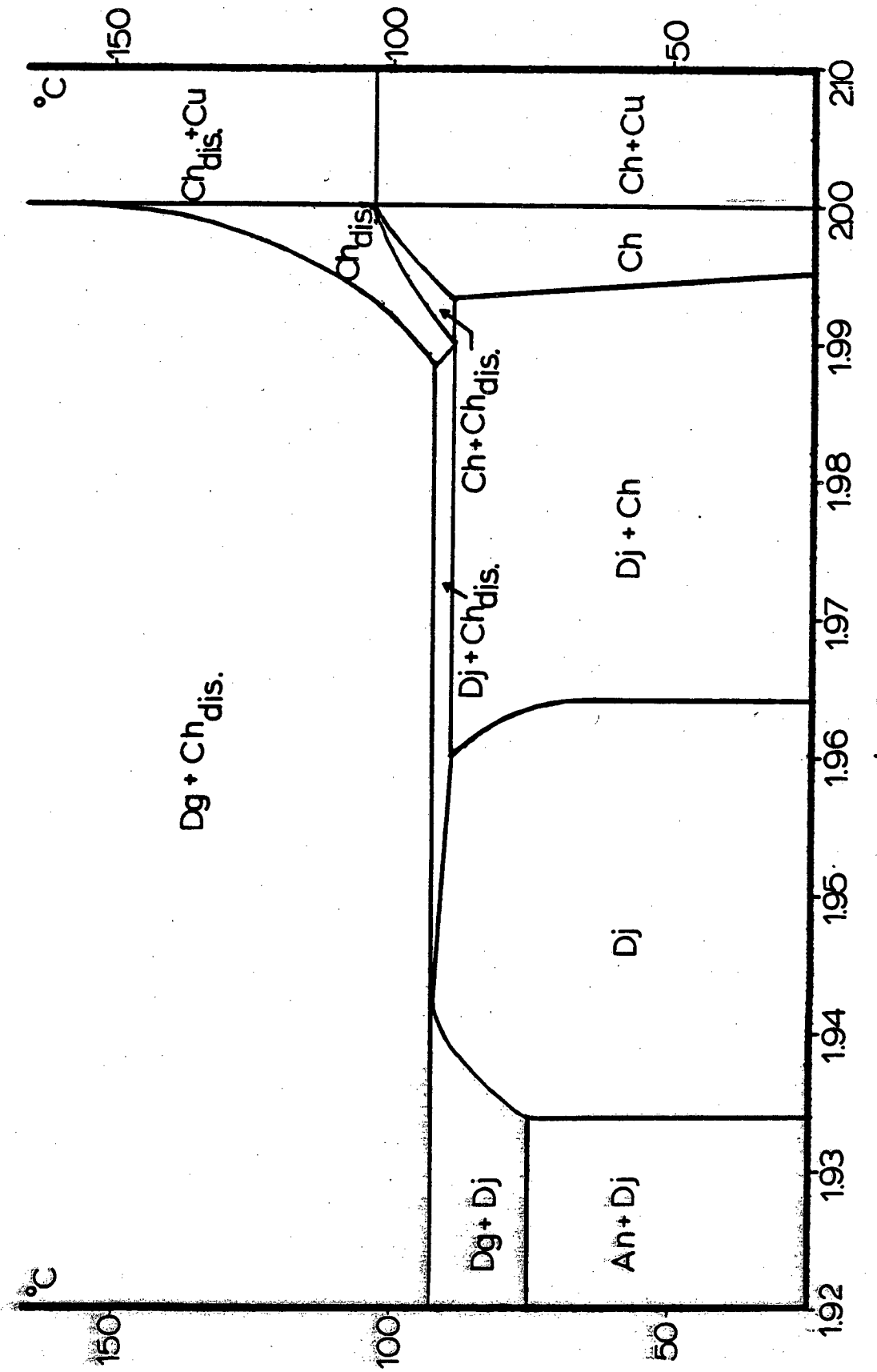
°C
150
100
50
Ch dis.+Cu
Ch+Cu
Ch dis.
Ch
Dg + Ch dis.
Ch+Ch dis.
Dj + Ch dis.
Dj + Ch
Dj
Dg + Dj
An + Dj
1.92
1.93
1.94
1.95
1.96
1.97
1.98
1.99
2.00
2.10
x in Cu x S
XBL 819-4928

Fig. 1

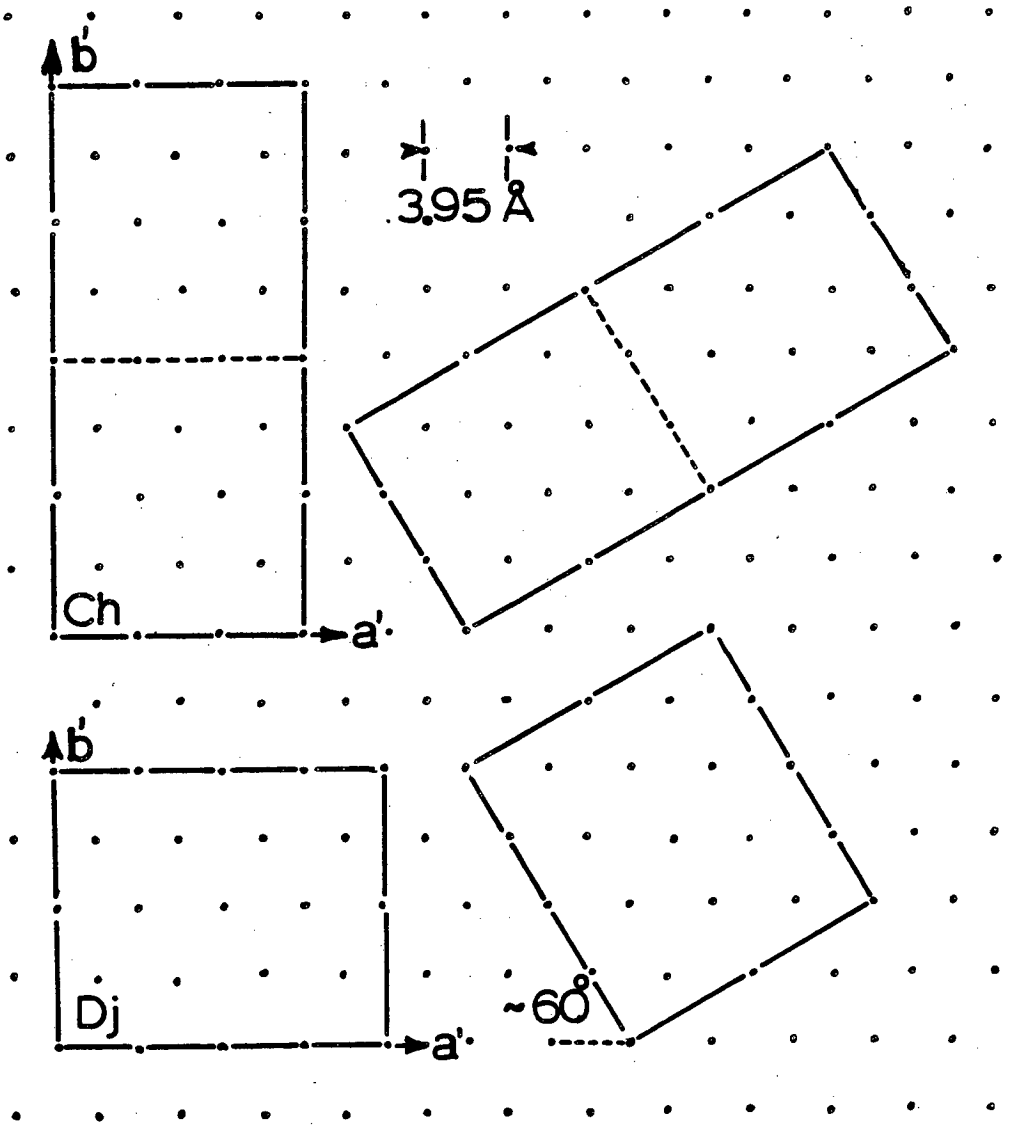

Chalcocite and Djurleite Unit Cells in the Basal Plane of the Sulfur Sublattice

XBL 819-7010

Fig. 2

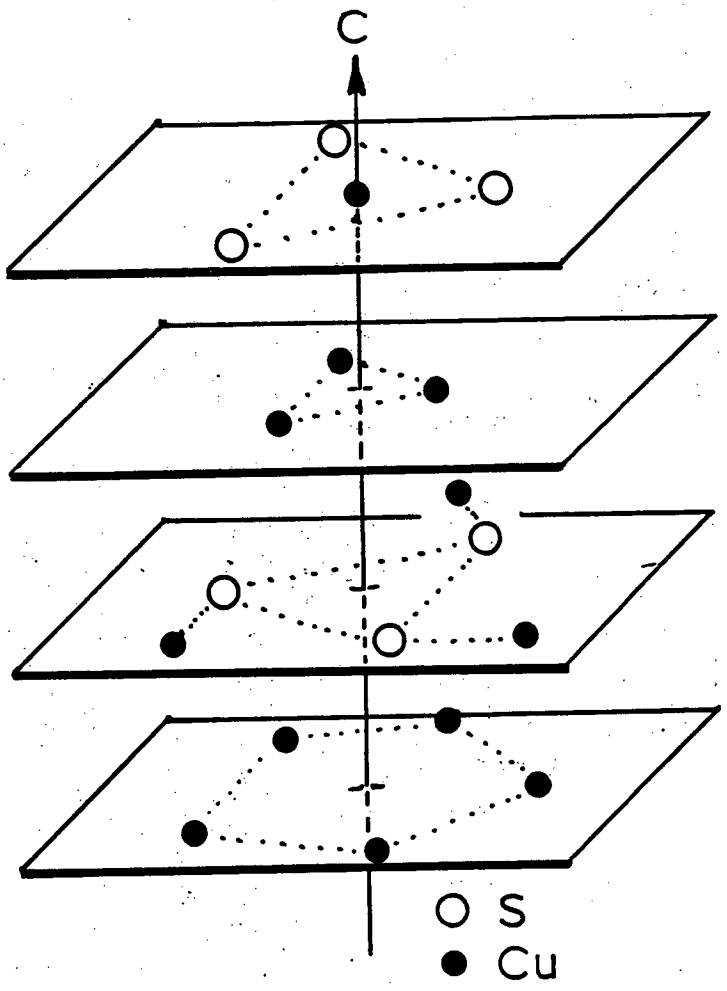

$Cu_{12}S_6$

Chalcocite Building Unit

XBL 819-7009

Fig. 3

THE ARRANGEMENT OF BUILDING UNITS IN CHALCOCITE

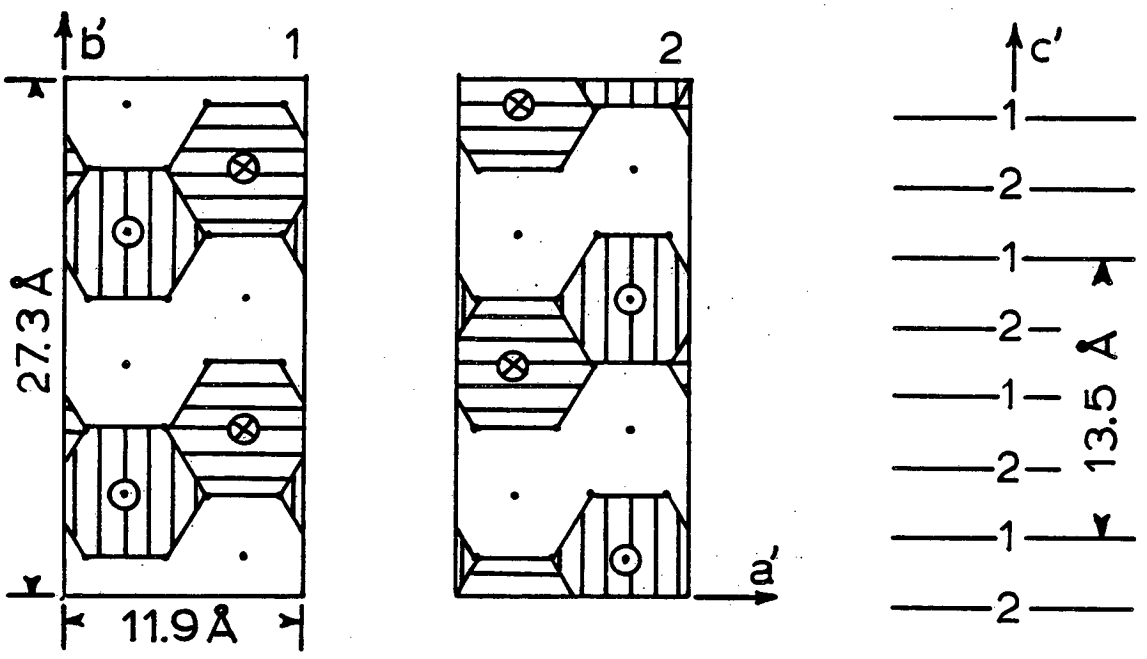

Hexagons represent the 5-Cu layers of the building units. The remainder of the unit is above (⊙) or below (⊗) the indicated plane.

XBL 8110-7087

Fig. 4

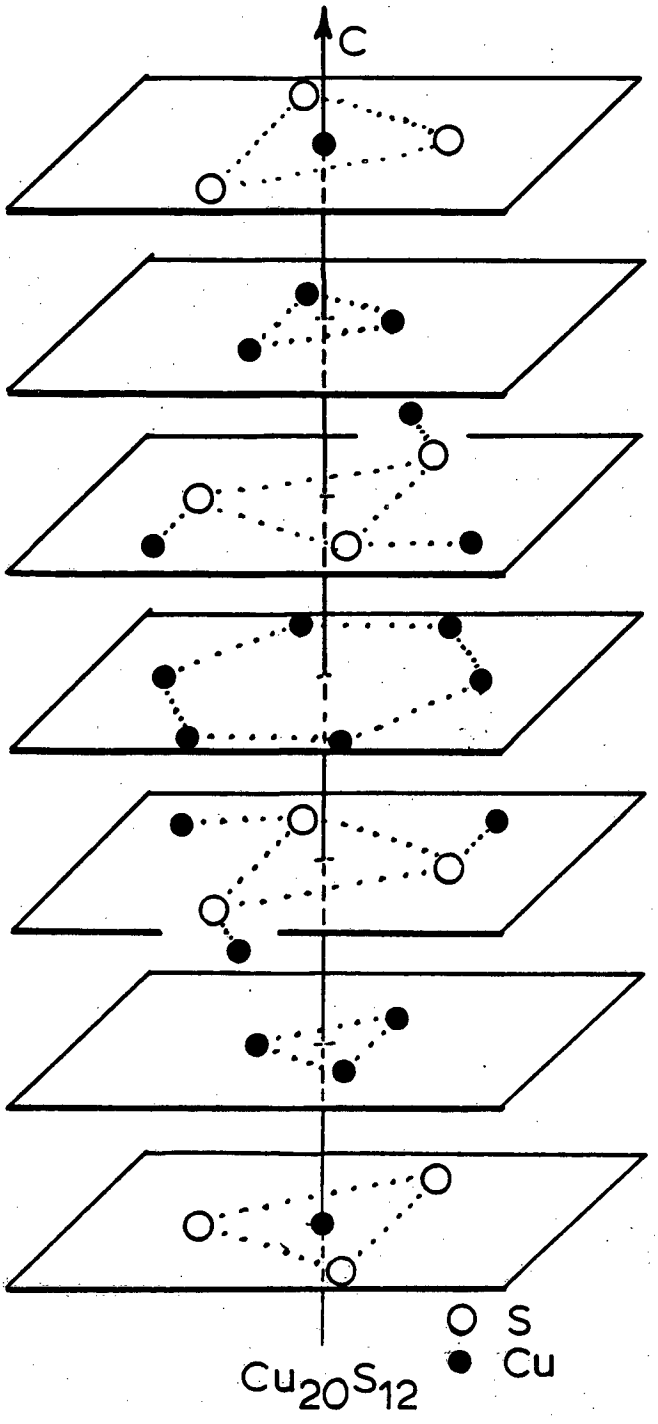

Djurleite: 4 Vacancy Cluster

Fig. 5

XBL 819-7008

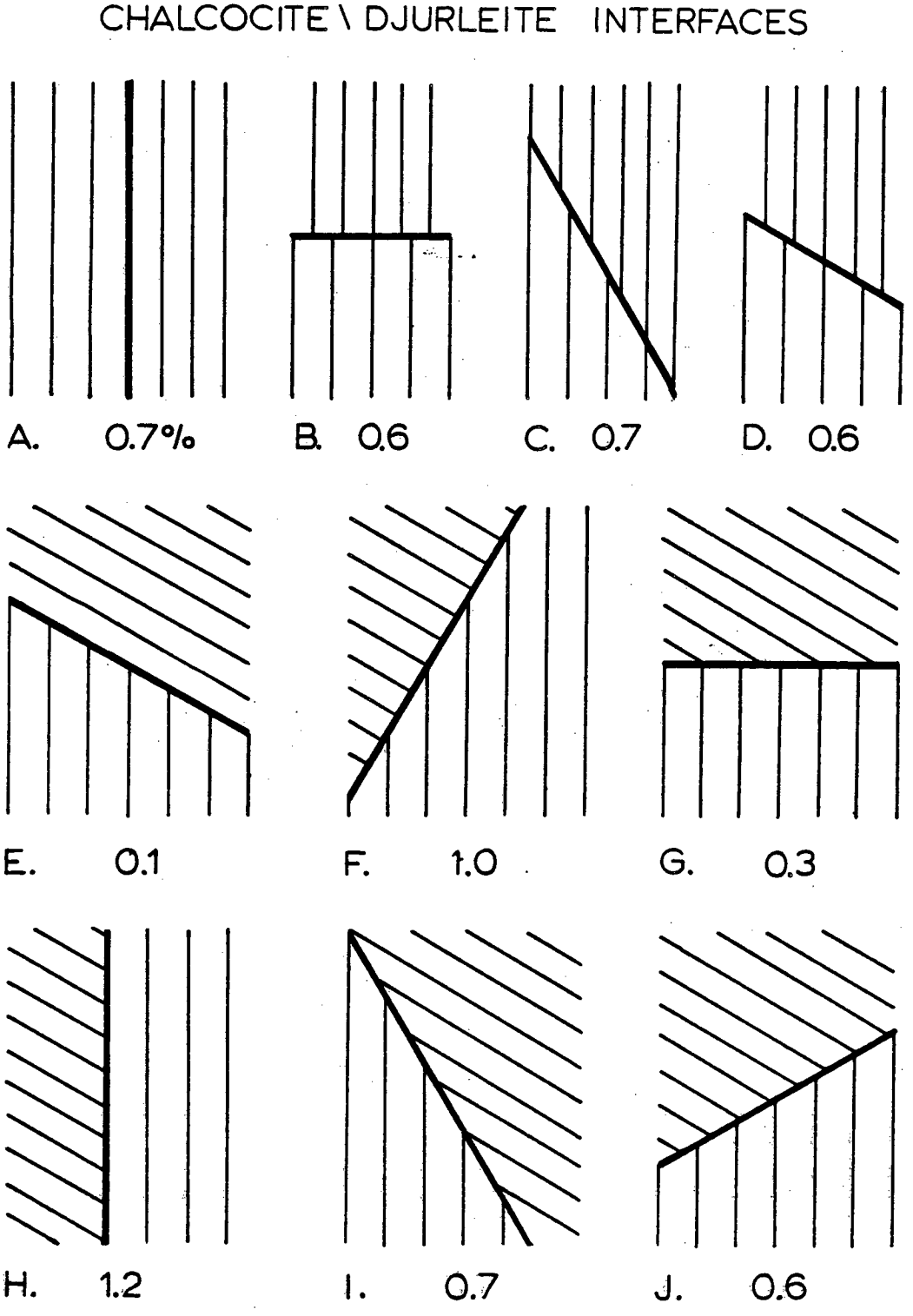

XBL 8110-7086

Fig. 6

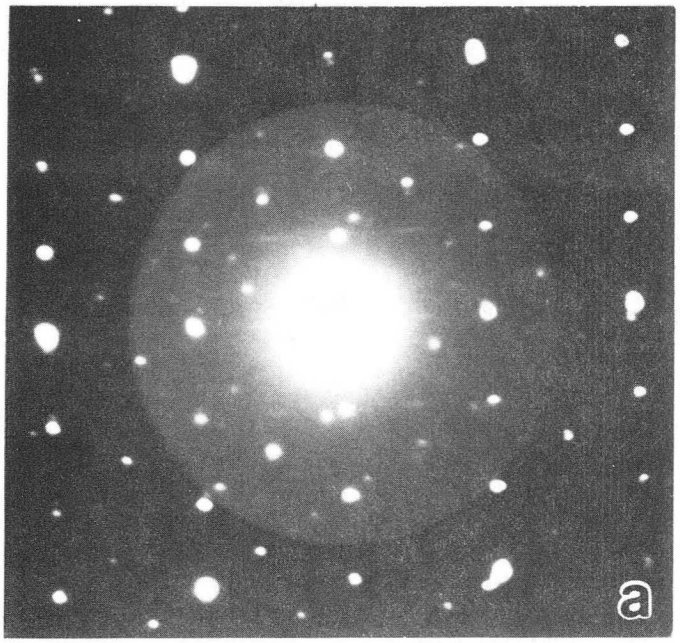

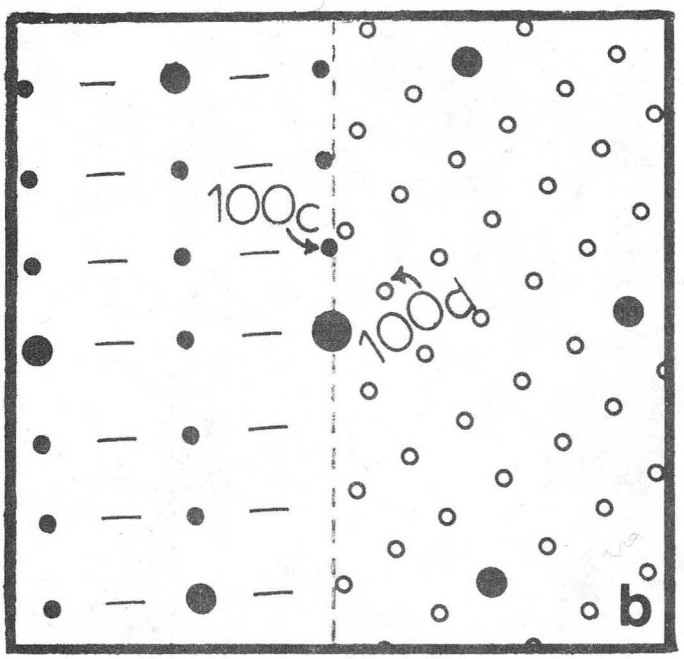

Chalcocite •
Djurleite ○
S sublattice ●

[001]

XBB 810-9595

Fig. 7a,b

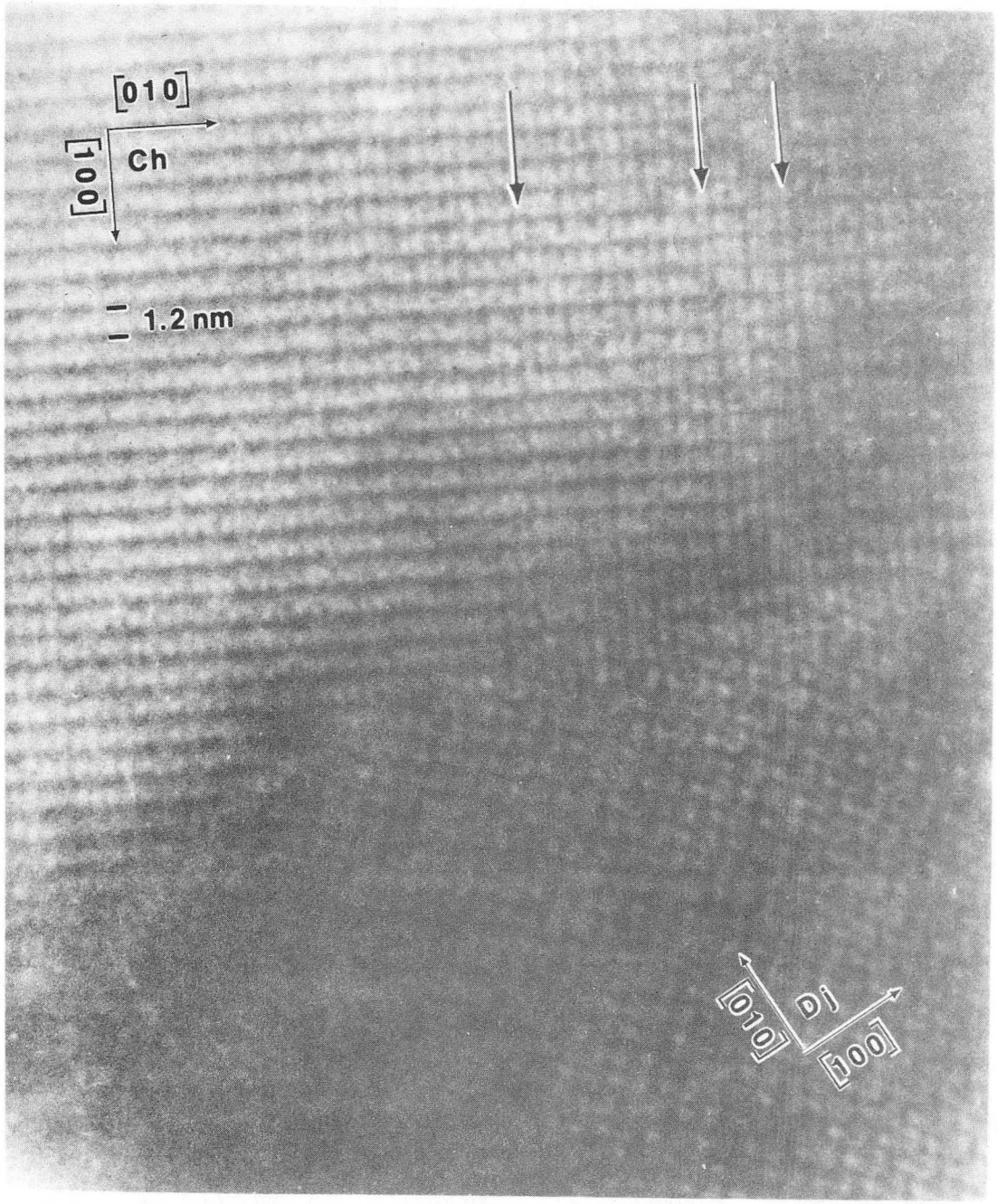

XBB 810-9275B

Fig. 7c

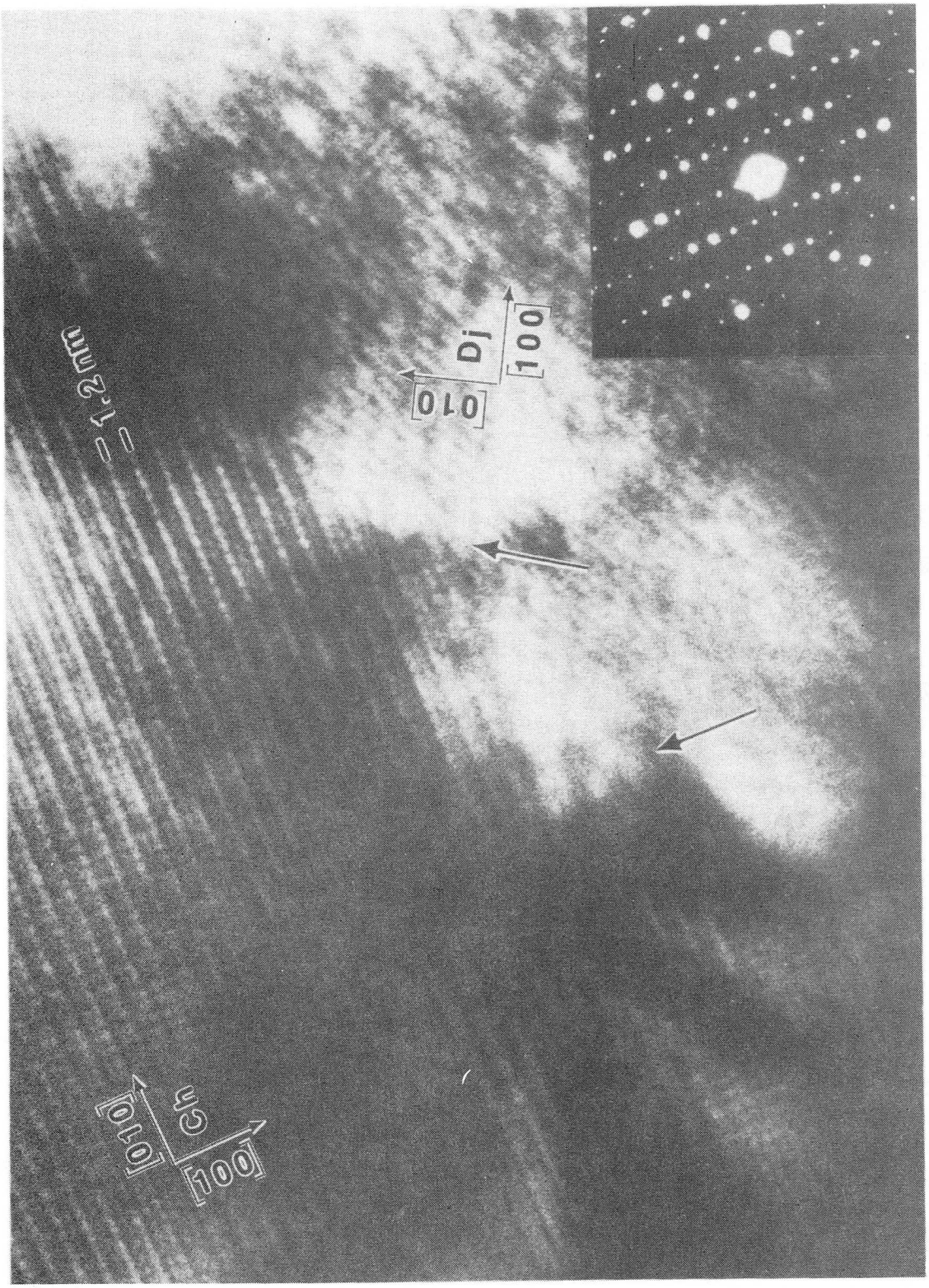

XBB 819-8918A

Fig. 8

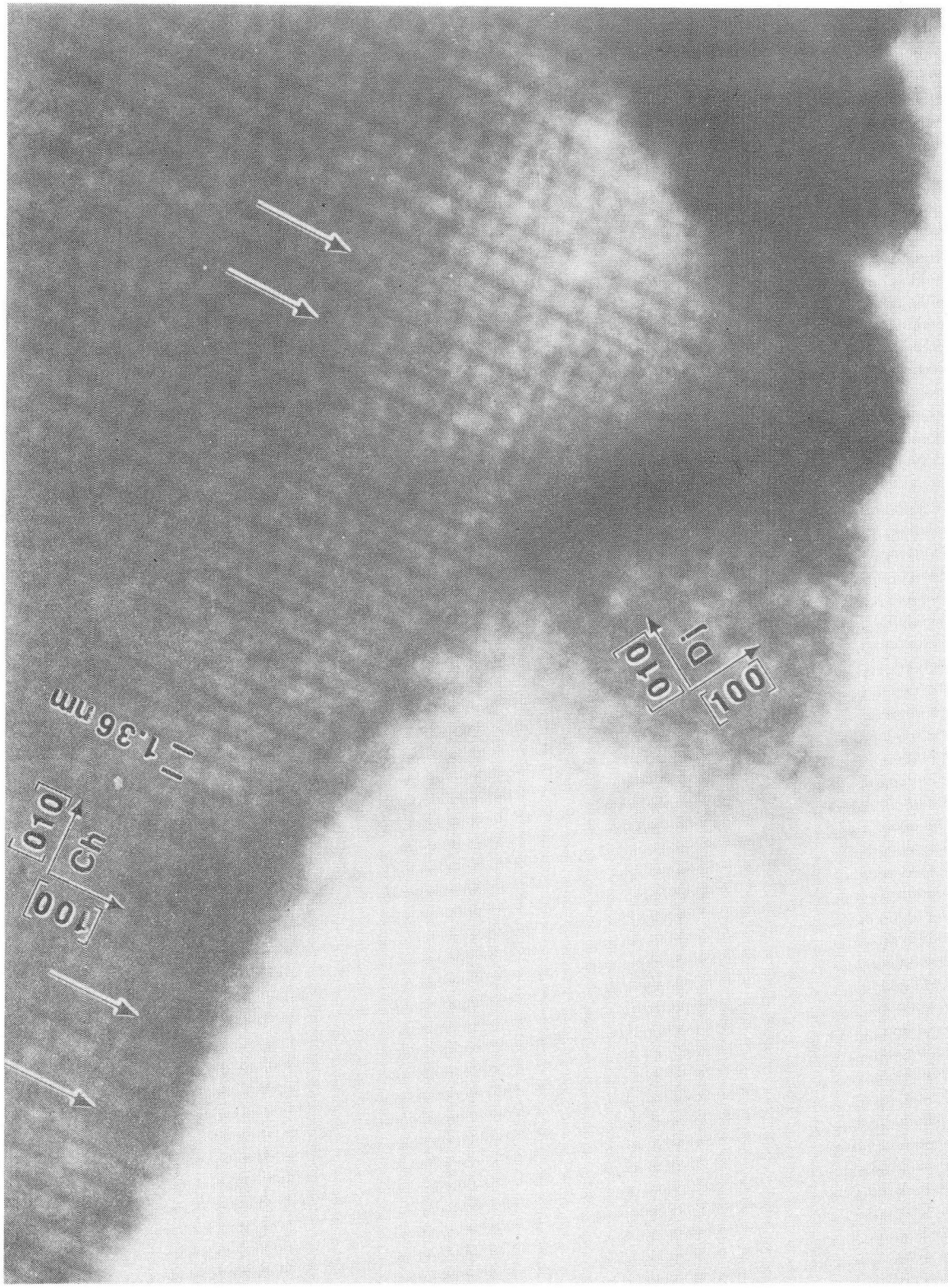

XBB 810-9274B

Fig. 9

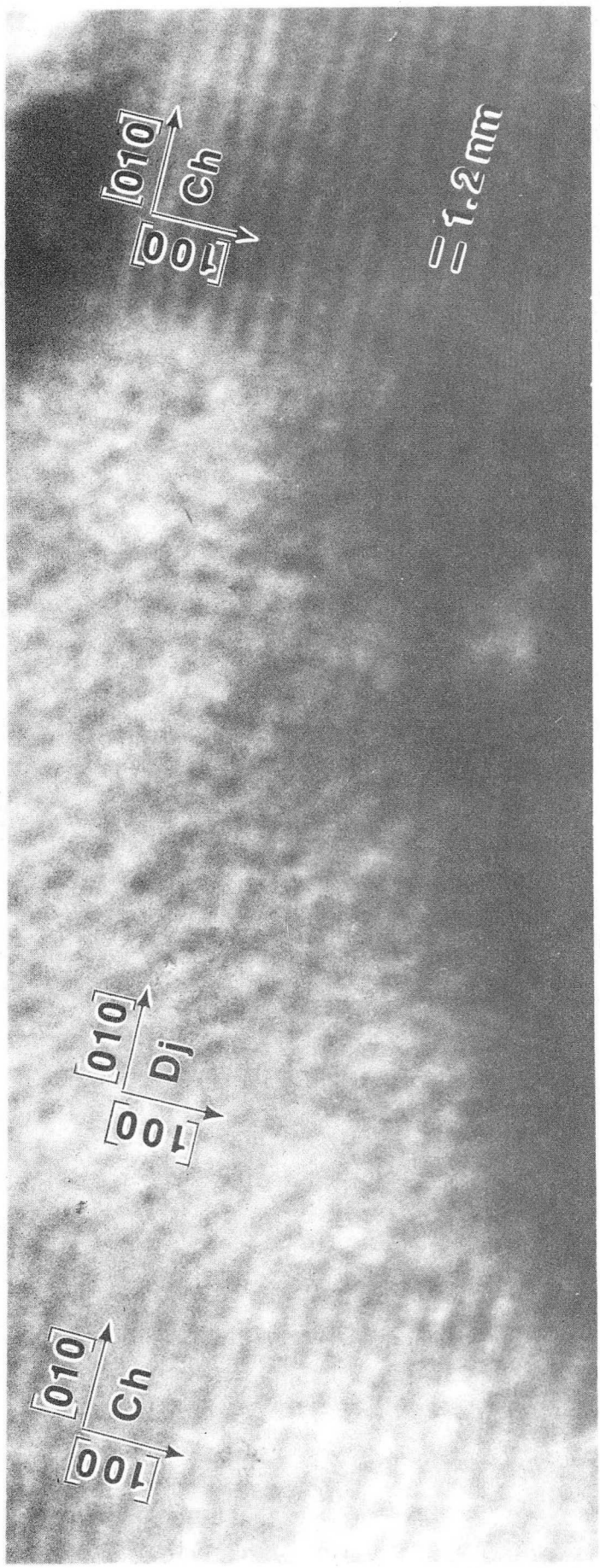

XBB 810-9595B

Fig. 10

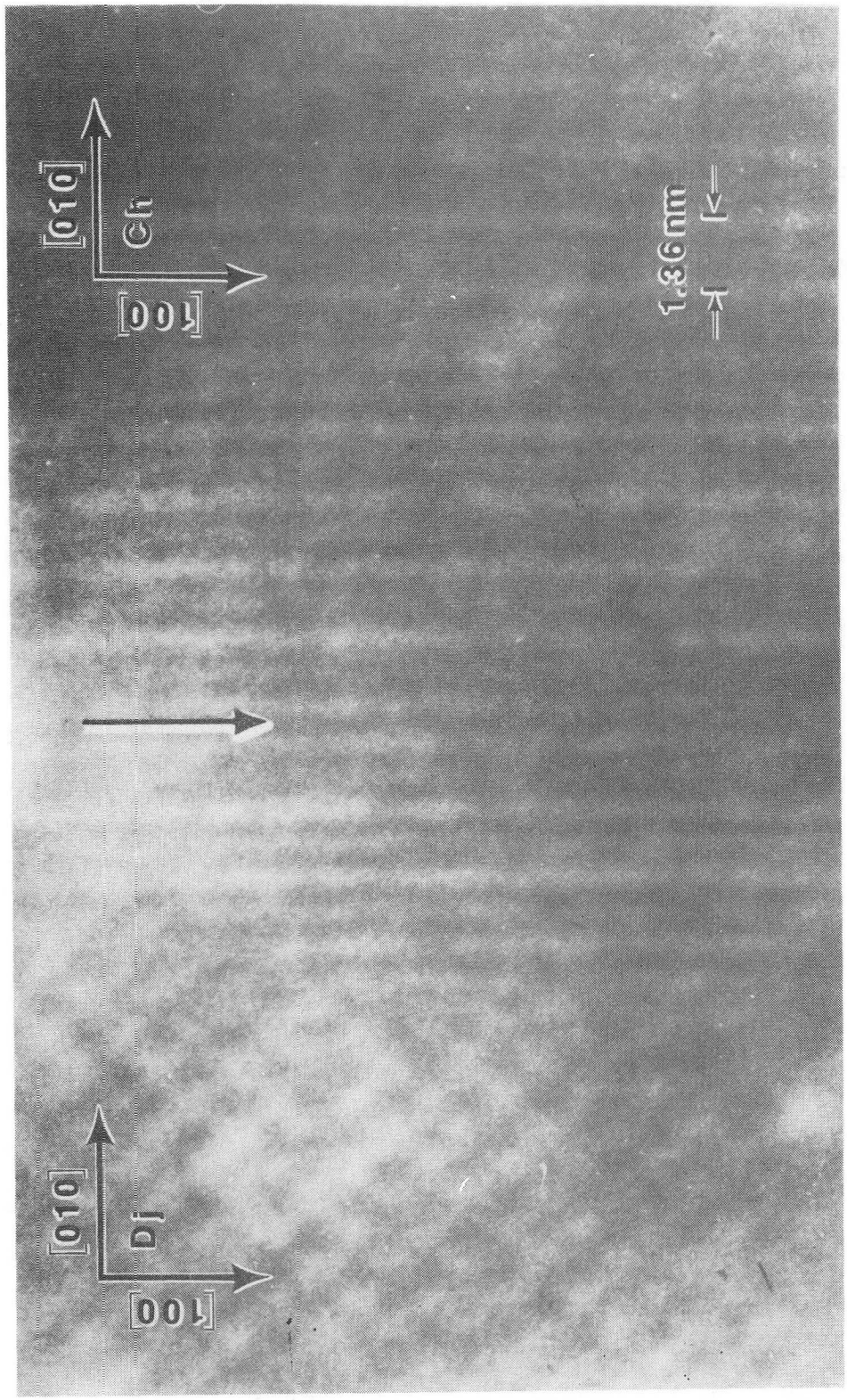

XBB 810-11440A

Fig. 11

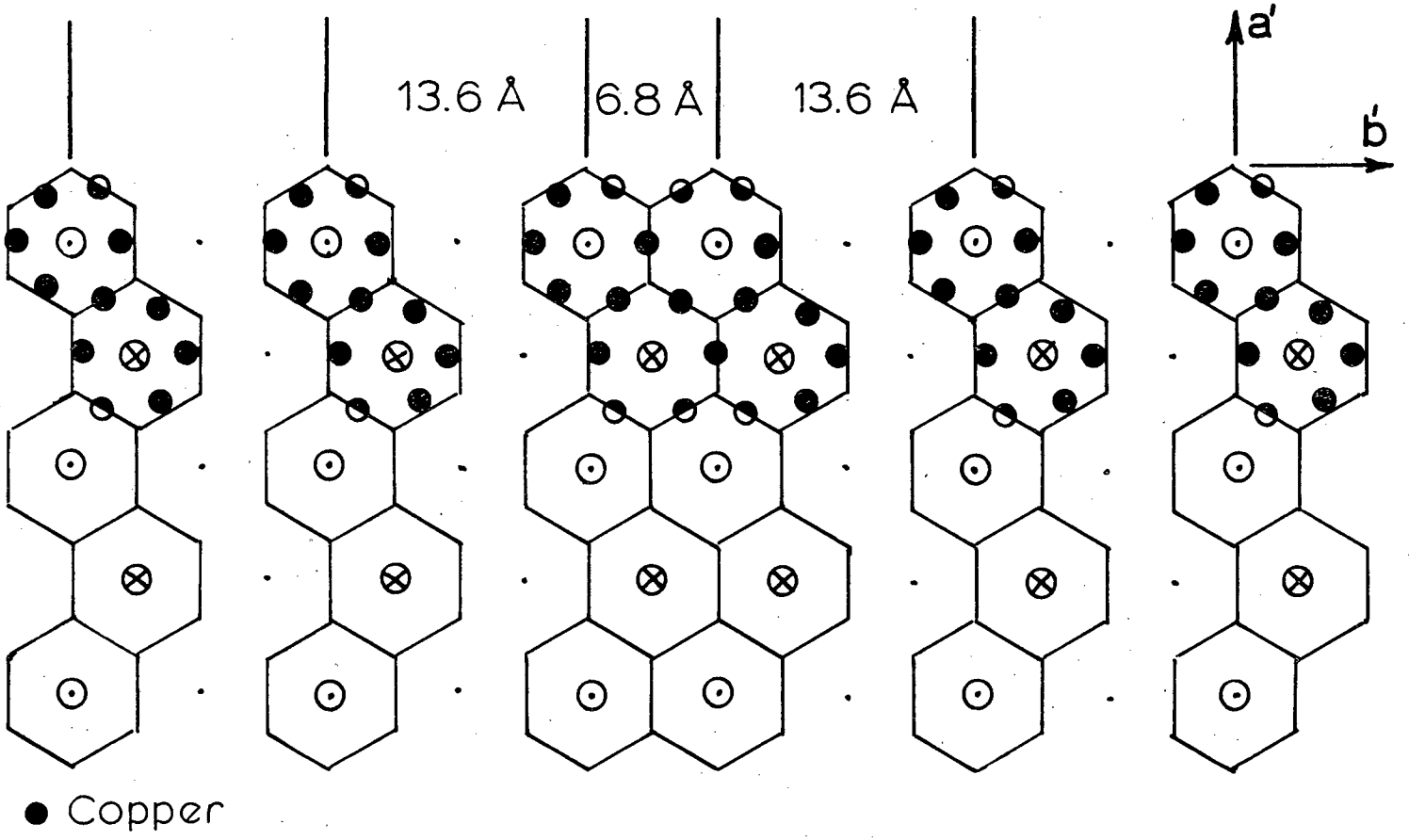

CHALCOCITE 1/4[010] FAULT

XBL 8110-11891

Fig. 12

TECHNICAL INFORMATION DEPARTMENT
LAWRENCE BERKELEY LABORATORY
UNIVERSITY OF CALIFORNIA
BERKELEY, CALIFORNIA 94720